Nanoscale

PAPER

View Article Online
View Journal | View Issue

Cite this: *Nanoscale*, 2014, **6**, 5532

Colloidal nickel/gallium nanoalloys obtained from organometallic precursors in conventional organic solvents and in ionic liquids: noble-metal-free alkyne semihydrogenation catalysts†

Kai Schütte,[a] Adinarayana Doddi,[b] Clarissa Kroll,[b] Hajo Meyer,[a] Christian Wiktor,[bc] Christian Gemel,[b] Gustaaf van Tendeloo,[c] Roland A. Fischer*[b] and Christoph Janiak*[a]

Efforts to replace noble-metal catalysts by low-cost alternatives are of constant interest. The organometallic, non-aqueous wet-chemical synthesis of various hitherto unknown nanocrystalline Ni/Ga intermetallic materials and the use of NiGa for the selective semihydrogenation of alkynes to alkenes are reported. Thermal co-hydrogenolysis of the all-hydrocarbon precursors [Ni(COD)$_2$] (COD = 1,5-cyclooctadiene) and GaCp* (Cp* = pentamethylcyclopentadienyl) in high-boiling organic solvents mesitylene and *n*-decane in molar ratios of 1 : 1, 2 : 3 and 3 : 1 yields the nano-crystalline powder materials of the over-all compositions NiGa, Ni_2Ga_3 and Ni_3Ga, respectively. Microwave induced co-pyrolysis of the same precursors without additional hydrogen in the ionic liquid [BMIm][BF$_4$] (BMIm = 1-butyl-3-methyl-imidazolium) selectively yields the intermetallic phases NiGa and Ni_3Ga from the respective 1 : 1 and 3 : 1 molar ratios of the precursors. The obtained materials are characterized by transmission electron microscopy (TEM), energy dispersive X-ray spectroscopy (EDX), IR, powder X-ray diffraction (PXRD) and atomic absorption spectroscopy (AAS). The single-source precursor [Ni(GaCp*)(PMe$_3$)$_3$] with a fixed Ni : Ga stoichiometry of 1 : 1 was employed as well. In comparison with the co-hydrogenolytic dual precursor source approach it turned out to be less practical due to inefficient nickel incorporation caused by the parasitic formation of stable [Ni(PMe$_3$)$_4$]. The use of ionic liquid [BMIm][BF$_4$] as a non-conventional solvent to control the reaction and stabilize the nanoparticles proved to be particularly advantageous and stable colloids of the nanoalloys NiGa and Ni_3Ga were obtained. A phase-selective Ni/Ga colloid synthesis in conventional solvents and in the presence of surfactants such as hexadecylamine (HDA) was not feasible due to the undesired reactivity of HDA with GaCp* leading to inefficient gallium incorporation. Recyclable NiGa nanoparticles selectively semihydrogenate 1-octyne and diphenylacetylene (tolan) to 1-octene and diphenylethylene, respectively, with a yield of about 90% and selectivities of up to 94 and 87%. Ni-NPs yield alkanes with a selectivity of 97 or 78%, respectively, under the same conditions.

Received 7th January 2014
Accepted 4th March 2014

DOI: 10.1039/c4nr00111g

www.rsc.org/nanoscale

Introduction

The properties of metals can be fine-tuned by alloying.[1,2] Bimetallic nanoalloys are particularly interesting for applications in colloidal and heterogeneous catalysis.[2–4] Bottom-up synthesis of such nanoalloys by soft, wet-chemical methods is of particular relevance in this respect.[5–7] Most studies on bimetallic systems are focussed on combinations of transition metals, typically involving noble metals which can easily be obtained by reduction from salt-like molecular precursors. Far less results are published on nanoalloys with electropositive Zn, Al, or Ga as components.[2,3] For example, Armbrüster *et al.* described the promising properties of PdGa, Pd_2Ga, Pd_3Ga_7 (ref. 8) and Fe_4Al_{13} (ref. 9) for alkyne semihydrogenation to alkenes instead of alkanes. Bridier *et al.* reported ternary

[a]*Institut für Anorganische Chemie und Strukturchemie, Heinrich-Heine-Universität Düsseldorf, 40204 Düsseldorf, Germany. E-mail: janiak@uni-duesseldorf.de; Fax: +49-211-81-12287; Tel: +49-211-81-12286*

[b]*Lehrstuhl Anorganische Chemie II – Organometallics & Materials, Ruhr-Universität Bochum, NC 2, Universitätsstr. 150, 44801 Bochum, Germany. E-mail: roland.fischer@rub.de; Fax: +49-234-321-4174; Tel: +49-234-32-24174*

[c]*EMAT, University Antwerp, groenenborgerlaan 171, 2020 Antwerp, Belgium. E-mail: staf.vantendeloo@ua.ac.be; Fax: +32-32-65-3318; Tel: +32-32-65-3262*

† Electronic supplementary information (ESI) available: Ni–Ga phase diagrams, EDX (XPS) of **NP1–NP8**, table of Ni : Ga ratios, TG of Ni–Ga SSPs, analysis of **NP4**, dec. of [Ni(GaCp*)$_3$(PCy$_3$)] with characterization, local resolution EDX of **NP3-IL**, Ni-NP characterization from Ni(COD)$_2$ and details of (semi-) hydrogenation catalysis. See DOI: 10.1039/c4nr00111g

Cu–Ni–Fe catalysts for semihydrogenation of propyne to propene with near 100% selectivity.[10] Selective (semi-)hydrogenation of alkynes to alkenes is of industrial and scientific interest, *e.g.*, to remove catalyst-poisoning acetylene traces from ethylene feeds.[11] Heterogeneous colloidal semihydrogenation catalysts typically contain noble metals[12] such as Pd,[13,14] Pt,[15] Ru,[16] Rh[17] and Au.[18] The usually high selectivity of semihydrogenation is still not understood completely,[13] but it is clear that total hydrogenation requires larger active sites than semihydrogenation[19] according to the site-isolation concept.[20] Hence a careful and perhaps fortuitous catalyst design involving alloying, Pd–C-phase formation,[21] and addition of promoters is necessary to achieve the desired semihydrogenation selectivity of the noble metal nano-catalysts together with high activity and catalyst stability. Compared to these established catalysts it seems that the Hume-Rothery type intermetallic compounds of type B metals (*i.e.* groups 2, 12 and 13) with low-cost transition metals are very promising novel materials in place of expensive noble-metal catalysts.

Previously we reported a non-aqueous organometallic synthesis of nano-brass (α/β-CuZn, γ-Cu_3Zn) by the co-hydrogenolysis of [CpCu(PMe_3)] and [ZnCp*$_2$] (Cp* = pentamethylcyclopentadienyl) or the co-decomposition of Cu- and Zn-amidinates {[Me(C(N^{i}Pr)$_2$)]Cu}$_2$ and [Me(C(N^{i}Pr)$_2$)]$_2$Zn as metal sources. This synthesis concept was used to prepare Cu/ZnO colloidal catalysts for methanol synthesis from $CO/CO_2/H_2$.[22,23] Our investigations of the related group-13 organometallic precursor chemistry showed that the low-valent [(AlCp*)$_4$] and the related GaCp* are valuable sources to obtain the intermetallic Hume-Rothery type nanoalloys of Co/Al, Ni/Al and Cu/Al by co-hydrogenolysis of the corresponding transition metal precursors.[24] Soft chemical synthesis in organic solvents from organometallic complexes is a means of access to chemical nanometallurgy and allows preparation of metals and alloys in the nanometer scale regime.[5,6]

Herein we present our results on the corresponding soft, wet-chemical synthesis of, to the best of our knowledge, hitherto unknown Ni/Ga nanoalloys using the individual metal-olefin precursors, [Ni(COD)$_2$] (COD = 1,5-cyclooctadiene) and GaCp* in appropriate ratios. We have also explored the hydrogenolysis of two single-source precursors with fixed Ni : Ga stoichiometry, [Ni(GaCp*)(PMe_3)$_3$] and [Ni(GaCp*)$_3$(PCy_3)]. In addition we compared this hydrogenolytic Ni/Ga nanoalloy synthesis in conventional organic solvents (*e.g.* mesitylene) with the synthesis in ionic liquids (ILs) using the same precursors, but without the need for additional hydrogen. ILs are well known for their unique properties for reaction control and for inherent stabilization of metal nanoparticles[25] which were prepared from metal salts,[26–29] organometallic metal complexes[30,31] and metal carbonyls.[32,33]

Nickel–gallium intermetallics

Group-13 metals (Al, Ga and In) readily form a number of different intermetallic compounds with nickel.[34] In the Ni–Ga system nine phases were characterized, Ni_3Ga, Ni_5Ga_3, Ni_3Ga_2 (HT), Ni_3Ga_2 (LT), NiGa, Ni_3Ga_4, Ni_2Ga_3, Ni_3Ga_7 and $NiGa_5$ (the latter two were previously believed to be $NiGa_4$) (Fig. S1 in the ESI†).[35] The NiGa phase melts congruently at 1220 °C.[33] The ternary phase Ni–Mg–Ga is of interest as a ferromagnetic shape-memory alloy also in nanoparticular form.[36] In general, nickel–gallium intermetallic phases and compounds are typically prepared by metallurgical processes, such as arc-melting followed by annealing at high temperatures for several weeks. Individual metals of high purity or the corresponding reducable metal salts serve as metal sources.[37] However, these procedures and precursors are neither suited for obtaining nanoalloy particles with much size control nor for free-standing (*i.e.* not agglomerated) nanoparticles dispersed in organic solvents (*i.e.* nanoalloy colloids).[6,38]

Therefore, we compare here the synthesis of Ni_xGa_y nanoalloy particles from organometallic precursors [Ni(COD)$_2$] and GaCp* or the single-source precursor [Ni(GaCp*)(PMe_3)$_3$] under different conditions. The phase NiGa is shown to be an effective catalyst for the semihydrogenation of alkynes.

Results and discussion

1. Nanocrystalline NiGa, Ni_2Ga_3 and Ni_3Ga powder samples by co-hydrogenolysis of [Ni(COD)$_2$] and GaCp* in mesitylene

Co-hydrogenolysis of GaCp* and [Ni(COD)$_2$] in various molar ratios in mesitylene under 4 bar H_2 pressure at 150 °C in the absence of any additional surfactants leads to immediate formation of a dark-red to brown solution.

The color gradually darkens and finally a black precipitate with a colorless (**NP1** and **NP3**) or brown (**NP2**) supernatant is formed (Scheme 1). The obtained insoluble products were characterized by means of powder X-ray diffraction (PXRD), bright-field transmission electron microscopy (BF-TEM), high-resolution TEM (HR-TEM), energy-dispersive X-ray spectroscopy (EDX), and atomic absorption spectroscopy (AAS) after digestion of a fraction of the respective sample. Fourier transform infrared spectroscopy (FTIR) proves the absence of any stabilizing organic moieties or hydrocarbon impurities. The PXRD patterns (Fig. 1) provide evidence for the formation of NiGa (**NP1**), Ni_2Ga_3 (**NP2**) and Ni_3Ga (**NP3**) which match the employed stoichiometric ratios of the reactants (Scheme 1). High resolution TEM images of all three samples (Fig. 1) confirm that the obtained materials are indeed nano-crystalline. **NP1** and **NP3** were proven to be NiGa and Ni_3Ga by indexing Fourier analyses of HR-TEM images of the corresponding samples (Fast Fourier Transformation, FFT, images of **NP1** and **NP3** in Fig. 1b are shown directly below in Fig. 1c). A high degree of agglomeration is observed, due to the absence of

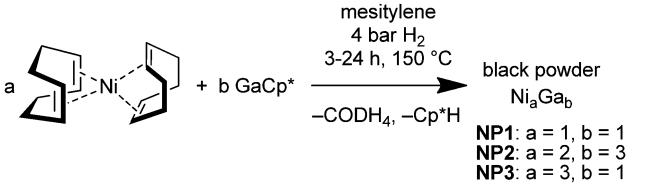

Scheme 1 Co-hydrogenolysis of [Ni(COD)$_2$] and GaCp* in mesitylene.

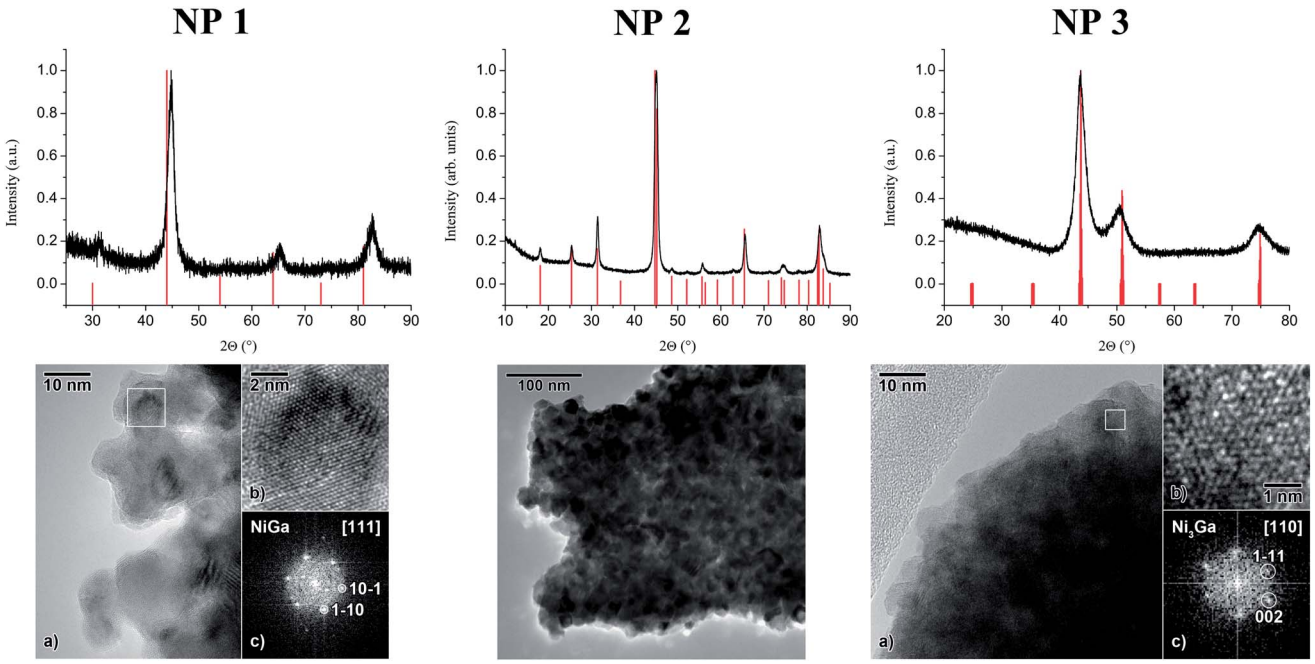

Fig. 1 PXRD, HR-TEM images and magnifications and FFTs of the respective areas marked by white squares of nanocrystalline Ni/Ga powder samples **NP1**, **NP2** and **NP3**. Reference data for PXRD and FFT indexation assignments were taken from ICSD no. 103854 (NiGa), 103860 (Ni_2Ga_3) and 103856 (Ni_3Ga).

any agents that could stabilize individual nanoparticles and their inherent superparamagnetic properties. EDX analyses (up to ±4% rel. error) of different agglomerates of **NP1** and **NP3** confirm the formation of rather pure NiGa and Ni_3Ga. **NP2** was found to be rather impure Ni_2Ga_3. Although the PXRD (Fig. 1) shows only reflections of the Ni_2Ga_3 phase, EDX spectra of different agglomerates of **NP2** yield different Ni/Ga ratios (Table S1 and Fig. S3–S5 in the ESI†). According to AAS reference data, the Ni and Ga molar ratios of the bulk samples are rather close to the expected values from TEM-EDX and correspond to the analytical compositions $Ni_1Ga_{1.07}$ (**NP1**), $Ni_2Ga_{3.08}$ (**NP2**) and $Ni_{2.79}Ga$ (**NP3**). If the overall composition derived from AAS is compared to the composition of individual agglomerated nanoparticles derived by EDX it is apparent that there are impurities of amorphous or hardly crystalline Ni and Ga in **NP2**. Notably, a reproducible shift to somewhat larger values of 2θ in the powder XRD pattern of **NP1** (assigned to the NiGa phase), suggesting significant contraction of the lattice parameters, is observed (Fig. 1). Such shifts in PXRD patterns are not uncommon for nanoparticles. A number of effects can be considered including a wide range of stoichiometric compositions, partly inhomogeneous element distribution, defects such as stacking and twin faults and nanosized crystalline domains being much smaller than the bulk reference material causing lattice contraction or expansion and strain.[39]

However, the shifts in the reflections for **NP1** are too high to be caused by a mere size effect of the crystalline domains. For **NP2** EDX shows a rather impure sample (see above). For **NP3** the width of the reflections is unreasonably large to be caused by small crystallites. Because of this and the high degree of agglomeration in the TEM images we conclude that calculation of the particle sizes for **NP1–3** from the PXRD patterns is not reasonable and will therefore not be presented here.

2. Hydrogenolysis of $[Ni(GaCp^*)(PMe_3)_3]$

A series of complexes $[Ni(GaCp^*)_x(PMe_3)_{4-x}]$ ($x = 1, 2$) can be synthesized from $[Ni(COD)_2]$, GaCp* and PMe_3 in the appropriate stoichiometric ratios.[40,41] The Ni_1Ga_1 complex $[Ni(GaCp^*)(PMe_3)_3]$ was chosen as a representative example in order to probe the validity of the single-source precursor (SSP) decomposition concept to accomplish the selective formation of the corresponding Ni_xGa_y phases (Scheme 2) and to compare this concept with the dual-source pathway (*vide supra*).

A yellow solution of $[Ni(GaCp^*)(PMe_3)_3]$ in *n*-decane was set under 4 bar H_2 pressure and heated to 185 °C for 60 h (Scheme 2; analytical data in the ESI†). The color of the solution gradually turns dark brown and the formation of a dark precipitate (**NP4**) is observed. The PXRD of **NP4** is in accordance with the pattern reported for the Ni_2Ga_3 phase and that observed for **NP2** (Fig. S10 in the ESI†). After annealing of the sample (20 h at 300 °C under a dynamic vacuum of 10^{-3} mbar) the reflections become sharper, but no phase transformation is observed.

The bright-field TEM images for **NP4** (Fig. S8 in the ESI†) show smaller particles (5−20 nm) as well as huge agglomerates

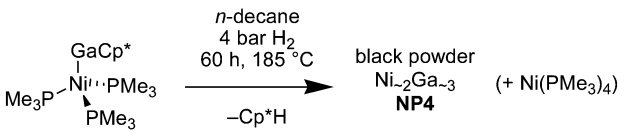

Scheme 2 Hydrogenolysis of the single-source precursor $[Ni(GaCp^*)(PMe_3)_3]$ in *n*-decane.

(up to several μm). The EDX data reveal substantial compositional variations with Ni : Ga ratios ranging between 1 : 1 to 1 : 2 (±10% rel. error) and point to the presence of amorphous impurities (Fig. S9†). The data were taken from larger areas of the sample, *i.e.* multiple particles. The AAS data agree with an overall ratio of 2 : 3 (*i.e.* $Ni_2Ga_{2.93}$) which matches with the expectation from the PXRD pattern (*vide supra*). The only crystalline phase present was identified as Ni_2Ga_3 (Fig. S10 in the ESI†) which proves that the impurities are amorphous. Interestingly, the observed Ni : Ga ratio is poor in nickel with respect to the precisely defined 1 : 1 stoichiometry of the single-source precursor starting material. The missing nickel forms $[Ni(PR_3)_4]$ as it was proven by a $^{31}P\{^1H\}$-NMR spectrum of the supernatant solution after the decomposition reaction. The spectrum shows one intense singlet peak at −21.78 ppm, which neither corresponds to free PMe_3 (−63.3 ppm) nor to the starting material (−5.6 ppm).[40] In fact, the observed chemical shift is very close to the one reported for the homoleptic PMe_3 complex of nickel, namely $[Ni(PR_3)_4]$ (−22.2 ppm).[41] This latter complex is surprisingly stable to hydrogenolysis under the applied conditions. It is noteworthy that the same effect occurs if a SSP with a sterically more demanding phosphine, *i.e.*, $[Ni(GaCp^*)_3(PCy_3)]$ is used (see Scheme S1, Fig. S11 and S12 in the ESI† for further information). Thus Ni/Ga SSPs should not contain phosphine ligands. However, a selective synthesis of suitable SSPs of the general formula $[Ni_a(GaCp^*)_bL_c]$ with $a/b = 1$, 2/3 or 3 and L being a more innocent ligand, which does not form stable nickel complexes as side products during hydrogenolysis, is still to be accomplished.

3. Colloidal Ni/Ga nanoalloy particles in mesitylene or *n*-decane

Based on the results of the above discussed co-hydrogenolysis of $[Ni(COD)_2]$ and GaCp* which led to nanocrystalline powder samples of rather controlled Ni/Ga phase compositions the same dual source precursor chemistry was employed to obtain colloidal solutions of the respective Ni/Ga nanoalloy particles. However, the organic reaction medium mesitylene or *n*-decane, respectively, did not prevent particle agglomeration. Therefore hexadecylamine (HDA) was chosen as an additive (surfactant). HDA is well known for reversible surface capping of metal and metal alloy nanoparticles and leads to the formation of rather stable colloidal solutions of non-agglomerated HDA-stabilized nanoparticles as it did here for the respective Ni/Ga nanoalloys. Notably, co-hydrogenolysis using dodecanethiol or polyphenylene oxide (PPO), *i.e.*, poly(oxy-2,6-dimethyl-1,4-phenylene), instead of HDA did not yield colloids, but black amorphous precipitates, which were not analyzed further. The as-synthesized HDA-stabilized particles were precipitated by addition of acetonitrile and were purified by washing with acetonitrile. The obtained samples **NP5–7** were characterized by the same techniques as **NP1–NP4**. BF-TEM images of **NP5–7** (Fig. 2) show individual particles of 5.0 nm (±1.3 nm standard deviation).

EDX measurements of **NP5–7** (Fig. S13a, S14 and S15a in the ESI†) indicate the formation of Ga-deficient materials with respect to the molar ratio of the precursors and the desired stoichiometry of the intermetallic phase. Thus, **NP5** (targeting NiGa) shows a Ni : Ga ratio between 1 : 0.54 and 1 : 0.73, **NP6** (targeting Ni_2Ga_3) shows a Ni : Ga ratio between 2 : 2.44 and 2 : 2.83 and **NP7** (targeting Ni_3Ga) shows a Ni : Ga ratio between 3 : 0.52 and 3 : 0.61 (Table S2a†). X-ray photoelectron spectroscopy (XPS) analysis of three different regions of two samples of **NP5** (targeting NiGa) gave Ni : Ga ratios between 1 : 0.68 and 1 : 0.91 and of **NP7** (targeting Ni_3Ga) gave Ni : Ga ratios between 3 : 0.39 and 3 : 0.78 (Fig. S13b, S15b and Table S2b in the ESI†).

Hydrogenation of the single-source precursor $[Ni(GaCp^*)(PMe_3)_3]$ in *n*-decane in the presence of HDA as a stabilizer results in colloidal NiGa particles **NP8**. According to EDX (Fig. S16 and Table S2a in the ESI†), the particles exhibit various compositions ranging from 1 : 0.2 to 1 : 1.77 and, hence, are not phase pure. A BF-TEM image (Fig. 2) shows particle sizes of 13 nm (±5 nm standard deviation).

Probably excess HDA reduces the amount of gallium in the resulting intermetallic Ni/Ga particles. It might form stable, soluble Ga(III) amino/amido/imido complexes or clusters by protolytic cleavage of Cp*H. At present, an analysis of the supernatant solutions after precipitation of the particles **NP5–7** by mass spectrometry and ^{1}H-NMR spectroscopy did not yield conclusive results. We did not study the phenomenon in great detail, because of the presented results in the next section.

According to BF-TEM images and EDX or XPS spectra all Ni/Ga materials synthesized in conventional solvents were either

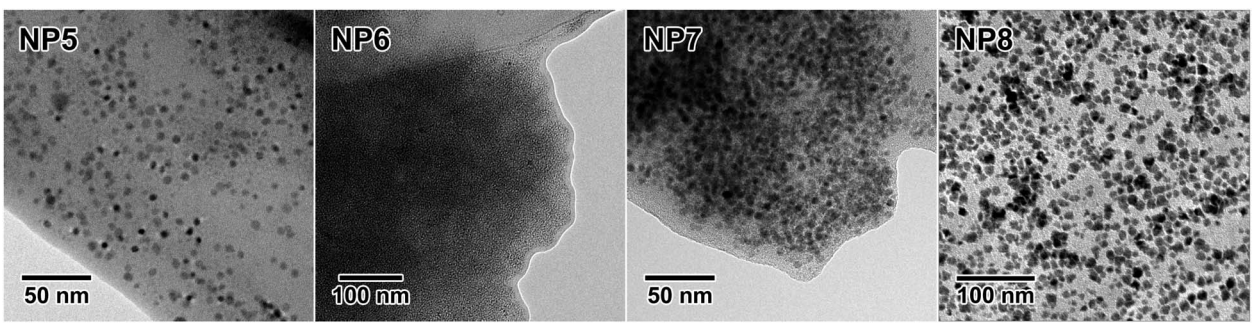

Fig. 2 BF-TEM images of HDA-stabilized colloidal mixed-phase Ni/Ga nanoalloys **NP5–7** obtained by co-hydrogenolysis of $[Ni(COD)_2]$ and GaCp* in mesitylene and of **NP8** from hydrogenation of $[Ni(GaCp^*)(PMe_3)_3]$ in *n*-decane.

heavily agglomerated or not phase pure. Thus, we refrained from further measurements.

4. Free-standing NiGa and Ni_3Ga nanoalloy particles obtained from $[Ni(COD)_2]$ and GaCp* in the ionic liquid $[BMIm][BF_4]$

Ionic liquids (ILs) are unique alternatives to conventional aqueous or organic solvents[42] and have been introduced to materials chemistry in particular over the last few years.[43,44] Using ILs for the bottom-up wet-chemical preparation of advanced functional materials, including metal nanoparticles, has been shown to be very promising.[45–49] The excellent solvation properties, high thermal stability, negligible vapor pressure, high ionic conductivity, and a broad liquid-state temperature range combined with the concomitant ionothermal synthesis method constitute particular advantages of ILs.[50,51] Microwave (MW) induced thermal decomposition of organometallic compounds in ILs is a rapid and energy-saving means of access to metal nanoparticles because of the significant absorption efficiency of ILs of microwave energy due to their ionic character, high polarity, and high dielectric constant.[52] In contrast to conductive heating, microwave radiation directly heats the reaction mixture and not primarily the vessel, *i.e.*, it is the reaction mixture which absorbs the microwave energy. This leads to localized superheating, very fast and efficient heating rates. The temperature of 200 °C is reached within seconds.[53–56] As soon as metal particles form from the thermally decomposed molecular precursors, they can absorb the MW radiation as well which leads to effective growth and annealing.

With these considerations in mind we investigated MW assisted co-pyrolysis of $[Ni(COD)_2]$ and GaCp* in 1 : 1 and 3 : 1 molar ratios in dried, deoxygenated $[BMIm][BF_4]$ without additional reduction by hydrogen. Quantitative decomposition of the precursors was achieved after only 10 minutes using a low power of 50 W at 220 °C in a nitrogen atmosphere (Scheme 3), which was verified by the complete absence of the characteristic $[Ni(COD)_2]$ peaks and the presence of the expected peaks of free COD in the ^1H NMR spectrum (Fig. S17 in the ESI†). Black colloidal solutions of 0.5 wt% of metal content were obtained. The respective samples are denoted as **NP1-IL** and **NP3-IL**. High-angle annular dark field scanning TEM (HAADF-STEM) yields characteristic diameters between 7 and 29 nm (average 14 ± 5 nm) for **NP1-IL** and between 12 and 19 nm (average 17 ± 4 nm) for **NP3-IL** (Fig. 3 and 4).

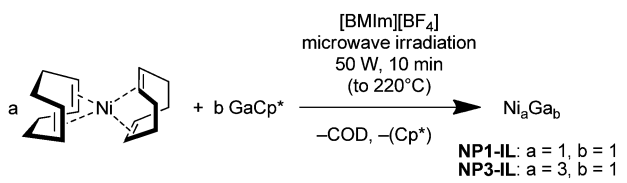

Scheme 3 Microwave (MW) induced thermal co-decomposition in the absence of H_2 in different molar ratios using the ionic liquid (IL) $[BMIm][BF_4]$ as the reaction controlling and particle stabilizing medium.

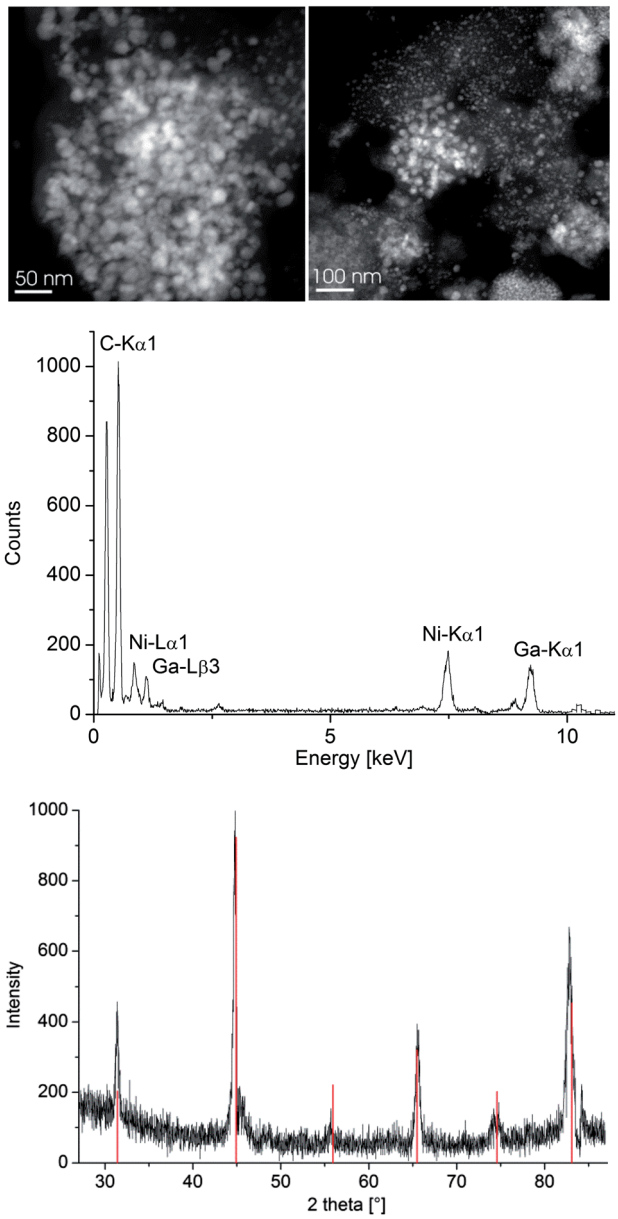

Fig. 3 HAADF-STEM image (top), EDX (middle), and PXRD (bottom) of NiGa nanoparticles **NP1-IL** in $[BMIm][BF_4]$. Reference data in red taken from ICSD no. 103854 (NiGa). Averaged particle composition (at.%) by EDX: Ni 49.2%; Ga 50.8% (Ni : Ga = 1 : 1).

In comparison to the agglomerated, nanocrystalline powder samples **NP1** and **NP3** obtained by co-hydrogenolysis from mesitylene, co-pyrolysis in an IL resulted in non-agglomerated nanoparticles. The Ni/Ga–IL dispersions are stable. Even after two weeks the NPs did not agglomerate, as it was shown by HAADF-STEM measurements carried out after this time.

Nanoparticles of **NP1-IL** were precipitated from the IL solutions by addition of a sufficient amount of acetone and characterized by PXRD providing evidence for NiGa as the single crystalline component. The slightly broadened reflections suggest crystallite domain sizes of 21 (±4 nm standard deviation) as calculated with the Scherrer equation.[57] It is noteworthy that the peaks in the PXRD of **NP1-IL** (Fig. 3) do not exhibit a

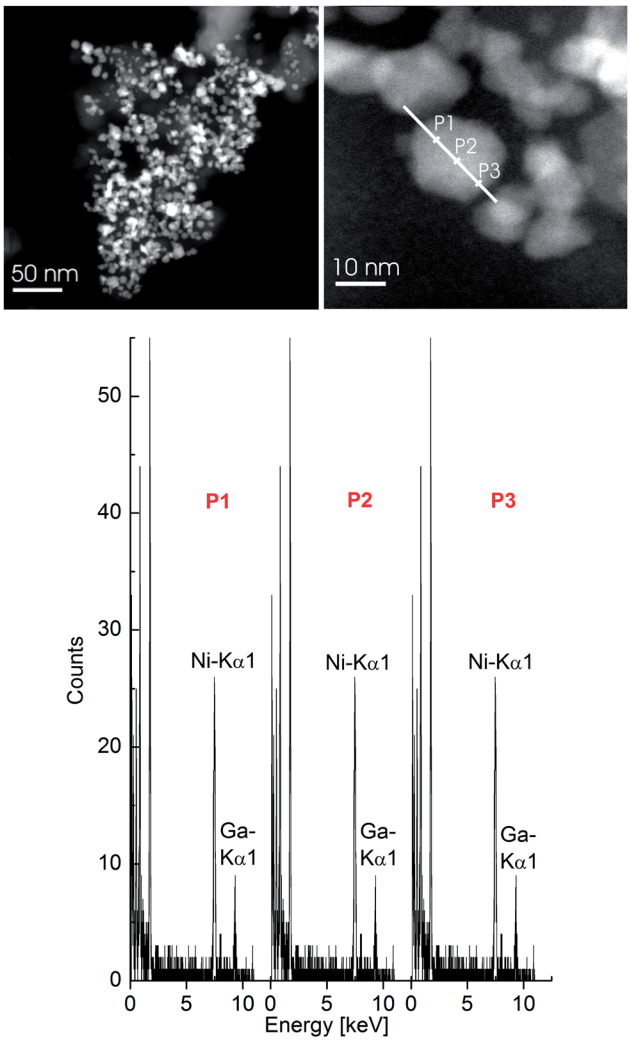

Fig. 4 HAADF-STEM images (top) and local EDX spectra (bottom) of **NP3-IL** recorded over an isolated particle along the white line (top right) with a 1 nm^2 spatial resolution and an acquisition time of 30 s. For additional points along the line see Fig. S18,† for an overview see Fig. 5.

significant shift in 2θ in comparison with the NiGa reference peaks, which was the case in the PXRD of **NP1** (Fig. 2). Interestingly, the pyrolysis and decomposition of both organometallic precursors occurred without hydrogenolysis by dihydrogen. This is somewhat surprising because of the quite robust nature of GaCp*. In conventional solvents GaCp* is thermally stable up to 300 °C (in the absence of hydrogen).[58] However, the reactivity of the imidazolium component of ILs with reactive metal centers has to be considered. It has been shown that in the course of metal nanoparticle formation from organometallic precursors in ILs, C–H/D activation/exchange processes may take place at molecular metal centers as well as at the surface of metal nanoparticles. Thus, nitrogen heterocyclic carbene species (NHCs) formed by decomposition of ILs may contribute to the stabilization of metal clusters and nanoparticles.[59] Hence, cooperative mechanisms involving H-transfer from the transition metal (*i.e.* Ni) to Ga and then the release of Cp*H need to be taken into account, even in the absence of additional hydrogen.[60]

The EDX spectra of **NP3-IL** for a single nanoparticle at different points as well as the average composition of 70–90 particles (Fig. 4 and 5) agree on a homogeneous phase of the composition Ni_3Ga. Fig. 4 illustrates EDX spectra at three (P1 to P3) out of six measured points (Fig. S18†) with 1 nm^2 resolution across a single nanoparticle with Ni 71 ± 5%; Ga 29 ± 5% (Ni : Ga ≈ 3 : 1) (larger instrumental errors due to a very small scan area).

Bimetallic nanoparticles can be differentiated into core–shell and alloy structures.[61] The formation of either structure depends on kinetic influences during metal reduction and nanoparticle growth processes as well as electron transfer processes between the metal species. For nano-alloy formation both metal precursor species must be reduced at the same rate and quantitatively. An inter-metal electron transfer of the type $M(1)^+ + M(2) \rightarrow M(1) + M(2)^+$ must be much slower to avoid metal segregation within a nano-cluster. The metal ratio of the formed alloy then corresponds to those of the precursors for quantitative reduction. The initial reduction according to $e^- + M^+ \rightarrow M$ followed by metal aggregation $M(1) + M(2) \rightarrow \{M(1)\ M(2)\}$ gives bimetallic nano-alloys.[61]

5. Catalytic semihydrogenation of alkynes with NiGa

The semihydrogenation of a C≡C triple bond to a C=C double bond is an important reaction in industrial and synthetic organic chemistry. Supported and modified noble (expensive) metal nanoparticles can be used in heterogeneous catalytic hydrogenation to prevent over-reduction to alkanes and to increase the stability of the catalyst.[8,13–18] Only a few reports were published on noble-metal-free heterogenous catalysts for alkyne semihydrogenation. These include nickel nanoparticles for the highly stereoselective *cis* semihydrogenation of internal alkynes[62] and Cu_3Fe and $Cu_{2.75}Ni_{0.25}Fe$ for the gas-phase semihydrogenation of propyne to propene.[9]

We have tested Ni-NPs (from $Ni(COD)_2$) and NiGa-NPs both in [BMIm][BF_4] under organic-solvent-free conditions for the (semi-)hydrogenation of 1-octyne (Scheme 4) and diphenylacetylene (Scheme 5).

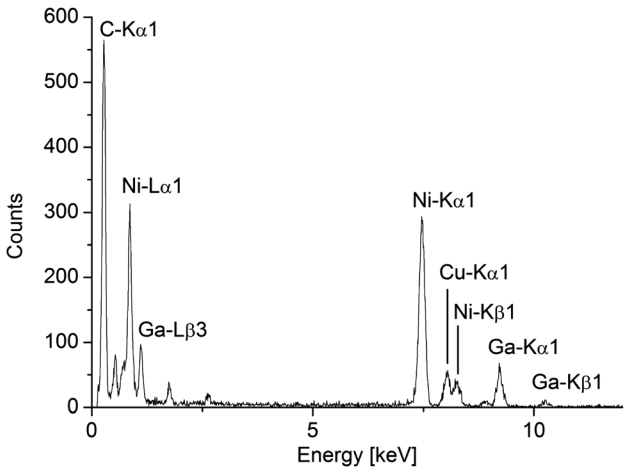

Fig. 5 EDX spectrum collected over 70–90 particles of **NP3-IL**.

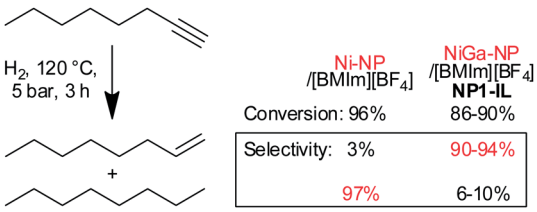

Scheme 4 Conversion rates and selectivity of the (semi-)hydrogenation of 1-octyne in the IL [BMIm][BF_4] by Ni-NPs and NiGa **NP1-IL**. **NP1-IL** was tested thrice with new NiGa samples (*cf.* Table 1).

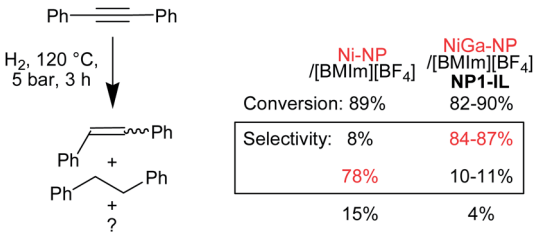

Scheme 5 Conversion rates and selectivity of the (semi-)hydrogenation of diphenylacetylene (tolan) in the IL [BMIm][BF_4] by Ni-NPs and NiGa **NP1-IL**. **NP1-IL** was tested twice. Diphenylethylene is a *cis–trans*-mixture.

Ni-NPs (median diameter 18 ± 6 nm, see Scheme S1, Fig. S19, S20 and Table S3 in the ESI†) showed high conversion rates for the total hydrogenation of the triple bond and selectivity to octane (97%) or diphenylethane (78%). On the other hand NiGa-NPs from **NP1-IL** yielded primarily 1-octene or diphenylethylene with 94% or up to 87% selectivity, respectively.

The NiGa catalyst can easily be recovered after product removal and re-used again with fresh substrate. The semi-hydrogenation of 1-octyne could be run four times with the same catalyst charge and little loss of conversion or selectivity (Table 1).

After catalysis the NiGa nanoalloy particles have increased in size to 68 (±10) nm but are still separate nanoparticles (Fig. 6).

Table 1 Semihydrogenation of 1-octyne with NiGa-NPs[a]

			Selectivity (%)	
Sample	Conversion (%)	TOF[b] [h^{-1}]	1-Octene	Octane
1	89	138	93	7
2	87	135	94	6
3a	89	138	92	8
3b	90	139	91	9
3c	88	136	90	10
3d	86	133	90	10

[a] In a typical catalytic test reaction 0.1 g NiGa/[BMIm][BF_4] dispersion (0.5 wt% = 0.005 g in total metal, 39 μmol NiGa) and 2 g (2.5 mL, 18.1 mmol) of degassed dry 1-octyne (molar NiGa : substrate ratio = 1 : 464) were stirred under 5 bar H_2 at 120 °C for 3 h. Runs 3a–3d were carried out with the same catalyst by removing the products in high vacuum at 50 °C. [b] TOF = mol product/(mol(NiGa, total metal) × time(h)).

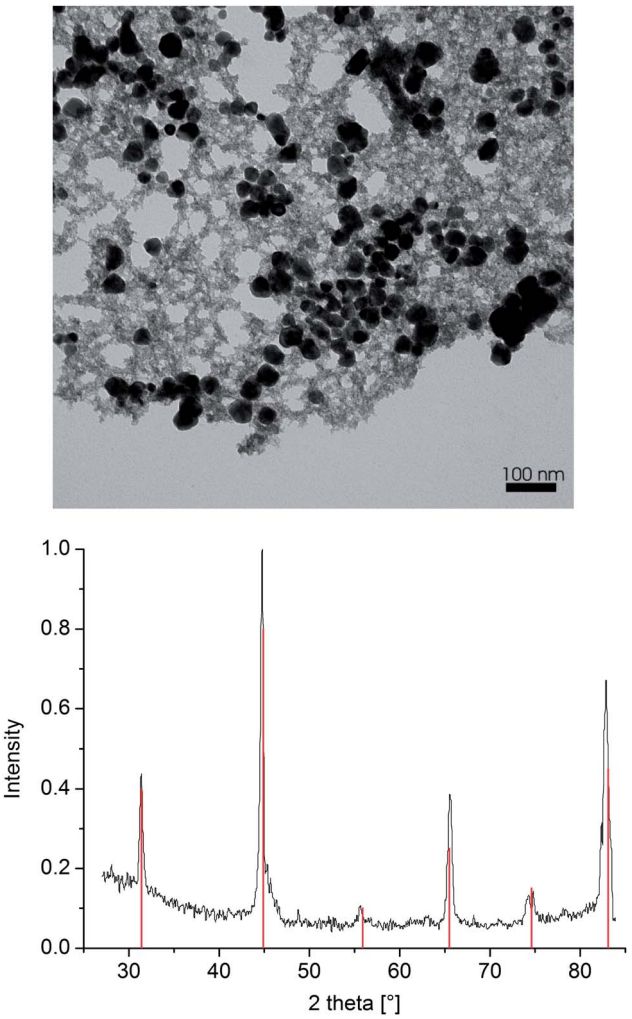

Fig. 6 TEM image (top) and PXRD (bottom) of NiGa-NPs after a 4th run with catalyst recycling (3d, Table 1) in the catalytic 1-octyne hydrogenation. PXRD reference data in red taken from ICSD no. 103854 (NiGa) (*cf.* Fig. 3 bottom).

PXRD confirms the unchanged presence of a crystalline NiGa phase in [BMIm][BF_4] after catalysis (Fig. 6).

Conclusions

We have investigated the soft wet-chemical preparation of nanocrystalline Ni/Ga alloy materials NiGa, Ni_2Ga_3, and Ni_3Ga in non-aqueous media. The dual source precursor concept based on the organometallic precursors [$Ni(COD)_2$] and GaCp* proved to be successful, while single-source precursors such as [$Ni(GaCp^*)(PMe_3)_3$] did not yield the expected Ni/Ga phase due to the formation of stable [$Ni(PMe_3)_4$] as a side product. Co-hydrogenolysis in the conventional organic solvent mesitylene turned out to be less reliable and selective in terms of yielding specific Ni_xGa_y phases than the co-pyrolysis conducted in the ionic liquid (IL) under microwave heating and in the absence of hydrogen. In particular, the reaction control and intrinsic particle stabilizing properties of ILs turned out to be advantageous, if non-agglomerated nanoalloy particles of

homogeneous composition and high crystallinity are the desired products. Very stable colloids of nanocrystalline NiGa and Ni_3Ga particles in the ionic liquid [BMIm][BF_4] were obtained. In contrast, in the case of co-hydrogenolytic preparation of the respective Ni/Ga colloids in conventional organic media, hexadecylamine (HDA) was needed as a surfactant additive. HDA turned out to be incompatible with the chemistry of GaCp* and caused undesired loss of the gallium component. Thus, the advantage of the ionic liquid as the reaction medium for nanoalloy synthesis is based on three aspects: (i) the non-necessity of H_2 and (ii) no additional surfactant is needed and (iii) the shorter reaction time (10 min *versus* several hours) with less energy consumed (50 W microwave energy focused on the sample *versus* several hundred Watts to heat an oil bath with a sample tube to 150 °C). From the precursor chemistry point of view the most attractive aspect might be the possible involvement of imidazolium CH activation and the formation of nitrogen heterocyclic carbene species in the course of the decomposition mechanism of the organogroup-13 precursor GaCp*. This aspect needs further investigations.

The synthesis of intermetallic Ni_xGa_y nanoparticles is a proof-of-concept for the easy and straightforward formation of nanoalloys from organometallic precursors in ILs. The catalytic NiGa semihydrogenation properties are further evidence that intermetallic Hume-Rothery phases of a metal from Cr–Ni and a metal from groups 12–15 can mimic and replace costly noble metal catalysts. Hume-Rothery type nanoalloys of Co/Al, Ni/Al and Cu/Al were already obtained by one of us by co-hydrogenolysis of the corresponding transition metal precursors.[22] The goal would be to obtain Fe/Al nanoalloys either from separate Fe and Al precursors or from Fe–Al mixed-metal clusters, such as [$Fe(AlCp^*)_5$].[63]

Experimental section

All experimental manipulations were performed under a purified inert nitrogen or argon atmosphere by using standard Schlenk line and glove-box techniques. Syntheses of **NP1–NP8** were carried out in 100 mL Fischer-Porter vessels. Syntheses of **NP1-IL** and **NP3-IL** were done in septum-sealed 10 mL CEM microwave-vessels in a CEM Discover microwave.

The solvents (acetone, acetonitrile, *n*-hexane, toluene, tetrahydrofuran) were dried using the MBraun solvent purification system. Mesitylene and *n*-decane were dried by passing the solvent over activated Al_2O_3 (neutral) column. The final H_2O content was controlled by Karl Fischer titration. The metal precursors $Ni(COD)_2$,[64] GaCp*,[65] and [$Ni(GaCp^*)(PMe_3)_3$][38] were prepared according to the previously reported procedures under strictly inert dry argon conditions. Poly(2,6-dimethyl-1,4-phenylene oxide) (PPO), hexadecylamine (HDA) and dodecanethiol were purchased from Acros Organics. HDA was dried and degassed prior to use.

The ionic liquid [BMIm][BF_4] was synthesized by reacting 1-methylimidazole with 1-chlorobutane to yield first [BMIm][Cl] which was further reacted with HBF_4 to give [BMIm][BF_4]. The IL was dried under high vacuum (10^{-7} mbar) at 80 °C for several days. Quantitative anion exchange and, thus, IL purity of >99% was assessed by ion chromatography (Dionex ICS-1100, with IonPac® AS14, 4 × 250 mm column). Water content measured by coulometric Karl Fischer titration (ECH/ANALYTIK JENA AQUA 40.00) was below 10 ppm.

Analytical techniques and instrumentation

Metal analysis was conducted at the laboratory of microanalysis of the Ruhr University Bochum (CHNSO: Vario EL by Elementar Hanau). AAS analysis for the metal content of Ga and Ni was undertaken using a Vario 6 AAS instrument from Analytik Jena. The samples were dissolved in *aqua regia* or HCl and H_2SO_4. NMR spectra were recorded on a Bruker Avance DPX-250 spectrometer (^1H, 250 MHz; ^{13}C, 62.9 MHZ; ^{31}P, 101.3 MHz) at 298 K in C_6D_6 and toluene-d_8 and the chemical shifts are referenced to the residual solvent peaks.

Powder X-ray diffraction (PXRD) data for the **NP1–NP8** samples were measured on a D8-Advance-Bruker-AXS-diffractometer (Cu-Kα-radiation, 1.54178 Å, scan step 0.0141° 2θ, heating current 30 mA) in Bragg–Brentano θ–2θ-geometry, using a Göbel mirror as a monochromator and a position sensitive detector. The powder samples were prepared under argon using Lindeman capillaries (diameter 0.5, 0.7 or 1.0 mm). The capillaries were flame-sealed prior to measurements. The detector was calibrated to the reflections of crystalline α-Al_2O_3. Measurements were done to collect the 2θ range of 10–90°.

PXRD data for **NP1-IL** and **NP3-IL** samples were measured at ambient temperature on a Bruker D2 Phaser using a flat sample holder and Cu-Kα radiation (λ = 1.54182 Å). Samples had been precipitated with acetone from the NP/IL dispersion and washed with acetonitrile.

TEM samples of **NP1–NP8** were prepared as diluted solutions or suspensions in toluene and deposited on carbon coated copper grids. Bright-field transmission electron microscopy (BF-TEM) images were acquired on a Philips CM30 equipped with a Schottky field emission gun (FEG) operating at 300 kV. BF-TEM together with energy-dispersive X-ray spectroscopy (EDX) were carried out using a Philips CM20 microscope equipped with a LaB_6 filament operating at 200 kV acceleration voltage and a Hitachi H-8100 microscope equipped with a LaB_6 filament operating at 200 kV acceleration voltage. BF-TEM, HR-TEM images, and EDX were acquired on a Tecnai FEI G2 microscope equipped with a FEG operating at 200 kV.

HAADF-STEM images of **NP-IL** samples were taken at room temperature using a Tecnai FEI G20 TEM equipped with a FEG operating at an accelerating voltage of 200 kV. Samples were deposited on 200 μm carbon-coated gold grids. The size distribution was calculated from a manual diameter determination over a minimum of 50 isolated particles.

All EDX spectra acquired in STEM mode were averaged scans over selected areas of ~100 × 100 nm^2. The EDX spectra of an isolated particle from **NP3-IL** were measured at several points with a spatial resolution of 1 nm^2 (acquisition time of 30 s at each point). Thereby the instrumental errors of this high-resolution EDX scan led to an estimated standard deviation of ±10–15% rel. error.

The X-ray photoelectron spectroscopy, XPS-(ESCA), measurement was performed with a Fisons/VG Scientific ESCALAB 200X XP-spectrometer, operating at room temperature, at a pressure of 1.0×10^{-8} bar and a sample angle of 30°. Using this spectrometer, electron spectra were recorded using polychromatic Al-Kα excitation (14 kV, 20 mA) and an emission angle of 0°. Calibration of the XPS was carried out by recording spectra, using Al-K_{alpha} X-rays, from clean samples of copper, silver and gold, at 20 eV and 10 eV pass energies and comparison with reference values.

GC/MS data were recorded on a Thermo Finnigan Trace DSQ.

Preparation of sample NP1 (NiGa)

In a Fischer-Porter vessel, 0.400 g of $[Ni(COD)_2]$ (1.454 mmol) and 0.296 g of GaCp* (1.450 mmol) were dissolved in mesitylene (15 mL). The resultant yellow-orange solution was degassed for 5 min and set to 4 bar H_2 pressure. The bottle was then placed into an oil bath at 150 °C. After 10 min of heating the solution became dark red, and slowly changed to dark brown after 20 min with the formation of a black precipitate. The mixture was stirred for 3 h at the same temperature, where upon the solution became colorless with a black precipitate. After cooling to room temperature (25 °C), the colorless supernatant was decanted under argon and the black material was washed several times with toluene (3 × 10 mL), followed by *n*-hexane (3 × 10 mL). The resultant material was dried under vacuum overnight at 50 °C. Yield: 0.184 g. AAS: Ni 39.69 wt% and Ga 50.27 wt%; n(Ni) : n(Ga) = 0.93. XRD reflections (2θ/°): 31.38, 44.85, 55.64, 64.45, 74.36 and 82.66. EDX analysis (±4% relative error): Ni 38 at.%; Ga 38 at.%; Ni : Ga = 1.0.

Preparation of sample NP2 (Ni_2Ga_3)

In a Fischer-Porter vessel, 0.600 g of $[Ni(COD)_2]$ (2.181 mmol) and 0.667 g of GaCp* (3.272 mmol) were dissolved in mesitylene (30 mL). The resultant yellow-orange solution was degassed for 3 min and set to 4 bar H_2 pressure. The bottle was then placed into an oil bath at 150 °C. The resultant clear red reaction mixture became dark red, then brown over a period of 15 min. After 30 min, formation of a black precipitate was observed. During the reaction a large drop in the hydrogen pressure had taken place. The reaction mixture was heated for 24 h, and cooled to room temperature. The resultant suspension was filtered to separate the black precipitate. This was then washed several times with toluene (4 × 20 mL), followed by *n*-hexane (3 × 20 mL) and dried under vacuum overnight. Yield: 0.273 g. AAS: Ni 32.54 wt% and Ga 59.52 wt%; n(Ni) : n(Ga) = 0.65; XRD reflections (2θ/°): 18.19 (0 0 1), 25.39 (1 0 0), 31.30 (1 0 1), 36.82 (0 0 2), 44.64 (2 −1 0), 45.23 (1 0 −2), 48.64 (2 −1 1), 52.26 (2 0 0), 55.69 (2 0 1), 56.45 (0 0 3), 59.30 (2 −1 2), 62.74 (1 0 3), 65.41 (2 0 2), 71.13 (3 −1 0), 73.99 (3 −1 1) and 74.75 (2 −1 3). Calculated particle size according to the Scherrer equation:[55] 3–6 nm.

Preparation of sample NP3 (Ni_3Ga)

Samples of 0.404 g of $[Ni(COD)_2]$ (1.469 mmol) and 0.100 g of GaCp* (0.489 mmol) were combined in a Fischer-Porter vessel in mesitylene (20 mL). The resultant yellow reaction mixture was degassed for 10 min at room temperature, set to 4 bar H_2 pressure and the Fischer-Porter vessel placed in an oil bath at 150 °C. After 5 min, the color of the reaction mixture changed to dark-brown, then after 15 min formation of a black precipitate was observed. The mixture was stirred for 6 h, where upon the solution became colorless. After cooling to room temperature the colorless supernatant was decanted under an argon atmosphere and the black material was washed several times with toluene (6 × 10 mL), followed by *n*-hexane (4 × 10 mL). Thereafter, the residual solvent and hydrocarbon byproducts were removed in vacuum and the black residue was thoroughly dried under vacuum overnight at 50 °C. Yield: 0.130 g. AAS: Ni 64.16 wt% and Ga 27.28 wt%; n(Ni) : n(Ga) = 2.79. XRD reflections (2θ/°): 43.68 (1 1 1), 50.52 (2 0 0) and 74.62 (2 2 0). EDX analysis (±4% relative error): Ni 46.6 at.%, Ga 15.3 at.%; n(Ni) : n(Ga) = 3.04.

Hydrogenolysis of $[Ni(GaCp^*)(PMe_3)_3]$ (sample NP4)

In a Fischer-Porter vessel, 1.140 g of $[Ni(GaCp^*)(PMe_3)_3]$ (2.326 mmol) was dissolved in *n*-decane (25 mL), pressurized with 4 bar H_2 and placed into an oil bath which was pre-heated to 185 °C. After 30 min of stirring at this temperature the colour of the solution changed to dark brown with slow formation of a black/brown precipitate. This mixture was further heated for 60 h. After cooling to room temperature, the suspension was transferred into a Schlenk tube and centrifuged to separate the black precipitate, which was then washed with *n*-hexane (5 × 20 mL) till all the washings were colourless and dried in vacuum. Yield: 250 mg. AAS: Ni 33.76 wt% and Ga 58.75 wt%. XRD reflections (2θ/°): 25.33 (100), 31.27 (101), 45.11(102), 48.63 (111), 52.16 (200), 55.47 (201), 62.92 (103), 65.57 (202), 71.06 (210), 74.48 (113).

Preparation of nickel–gallium colloidal nanoparticles (NP5)

In a Fischer-Porter vessel, 0.200 g of $[Ni(COD)_2]$ (0.727 mmol), 0.148 g of GaCp* (0.725 mmol) and dry HDA (hexadecylamine) (0.098 g, 0.407 mmol) were dissolved in mesitylene (7 mL). The resultant yellow-orange solution was degassed for 5 min and set to 4 bar H_2 pressure. The bottle was then placed into an oil bath at 150 °C. After 10 min of heating the solution changed to dark brown/black. The mixture was stirred for 3 h at the same temperature. After cooling to room temperature (25 °C), the stabilized black particles were precipitated by dry acetonitrile and washed three times with dry acetonitrile (7 mL) by ultrasonic treatment and centrifugation. After this the black material was suspended in dry toluene (10 mL). Yield: 0.112 g. EDX analysis (±0.26% relative error): Ni 61.93%; Ga 38.06% (*k*-factors: Ni 1.511, Ga 1.934).

Preparation of nickel–gallium colloidal nanoparticles (NP6)

In a Fischer-Porter vessel, 0.300 g of $[Ni(COD)_2]$ (1.091 mmol), 0.222 g of GaCp* (1.083 mmol) and dry HDA (hexadecylamine) (0.395 g, 1.637 mmol) were dissolved in mesitylene (7 mL). The resultant yellow-orange solution was degassed for 5 min and set to 4 bar H_2 pressure. The bottle was then placed into an oil bath at 150 °C. After 10 min of heating the solution changed to dark

brown/black. The mixture was stirred for 24 h at the same temperature. After cooling to room temperature (25 °C), the stabilized black particles were precipitated by dry acetonitrile and washed three times with dry acetonitrile (7 mL) by ultrasonic treatment and centrifugation. The washing solution was decanted every time. After this the black material was suspended in dry toluene (10 mL). Yield: 0.184 g. EDX analysis (Ni ±0.41%, Ga ±0.64% relative error): Ni 37.36%; Ga 62.36% (*k*-factors: Ni 1.511, Ga 1.934).

Preparation of nickel–gallium colloidal nanoparticles (NP7)

In a Fischer-Porter vessel, 0.150 g of $[Ni(COD)_2]$ (0.545 mmol), 0.037 g of GaCp* (0.181 mmol) and dry HDA (hexadecylamine) (0.197 g, 0.818 mmol) were dissolved in mesitylene (7 mL). The resultant yellow-orange solution was degassed for 5 min and set to 4 bar H_2 pressure. The bottle was then placed into an oil bath at 150 °C. After 10 min of heating the solution changed to dark brown/black. The mixture was stirred for 6 h at the same temperature. After cooling to room temperature (25 °C), the stabilized black particles were precipitated by addition of dry acetonitrile and washed three times with dry acetonitrile (7 mL) by ultrasonic treatment and centrifugation. The washing solution was decanted every time. After this the black material was suspended in dry toluene (10 mL). Yield: 0.074 g. EDX analysis (Ni ±0.36%, Ga ±0.16% relative error): Ni 84.47%; Ga 15.25% (*k*-factors: Ni 1.511, Ga 1.934).

Preparation of nickel–gallium colloidal nanoparticles (NP8)

A Fischer-Porter vessel was charged with 0.500 g $[Ni(GaCp^*)(PMe_3)_3]$ (1.016 mmol) and 1.227 g dry HDA (hexadecylamine) (5.052 mmol). To this reaction mixture *n*-decane (20 mL) was added. The resultant yellow reaction mixture was degassed for 15 min at, set to 4 bar H_2 pressure and the Fischer-Porter vessel was placed in an oil bath at 185 °C. After 10 min the mixture became brown, then dark brown without the formation of any precipitate. The mixture was then heated for 15 h. The resultant reaction mixture was cooled to room temperature and the dark brown solution was transferred into a Schlenk tube. Dry ethanol (100 mL) was added and stirred for 2 h. The resulting cloudy solution was centrifuged to get a dark brown semi-solid. This was then washed with dry methanol, followed by ethanol (2 × 20 mL) and dried under vacuum for 3 days. Yield: 32 mg. IR (ν, cm^{-1}, neat): 3245 (vw), 3115 (vw), 2935 (vs), 2894 (vs), 2826 (vs), 1588 (w), 1454 (w), 1397 (w), 1249 (vs), 1080 (s), 1008 (vs), 860 (w), 791(vs), 713 (w), 681 (w). DLS (in dry toluene): 12–40 nm particle size. XRD reflections ($2\theta/°$): 31.38, 38.01, 45.21, 44.75, 48.71, 57.21, 62.87, 65.66 and 70.26.

Preparation of sample NP1-IL (NiGa colloid in an ionic liquid)

Co-decomposition of $[Ni(COD)_2]$ (13.3 mg, 0.048 mmol) and GaCp* (9.9 mg, 0.048 mmol) by means of microwave irradiation was carried out under nitrogen. In a typical reaction, the precursor powders were dissolved/suspended under a nitrogen atmosphere at room temperature in dried and deoxygenated $[BMIm][BF_4]$ (1 mL, density $[BMIm][BF_4]$: 1.21 g mL^{-1}, 1.21 g) for a 0.5 wt% M-NP/$[BMIm][BF_4]$ dispersion. For the synthesis, the mixture was placed in a microwave (CEM, Discover) under an inert nitrogen atmosphere and the conversion was finished within 10 min at a power of 50 W and a temperature of 220 °C. Each decomposition reaction was carried out at least twice. XRD reflections ($2\theta/°$): 31.4, 44.9, 55.9, 65.5, 74.6 and 83.3. EDX analysis (±1.7% relative error): Ni 49.0%; Ga 51.0% (*k*-factors: Ni: 1.511, Ga: 1.934).

Preparation of NP3-IL (Ni_3Ga colloid in an ionic liquid)

The co-decomposition of $[Ni(COD)_2]$ (13.5 mg, 0.049 mmol) and GaCp* (3.3 mg, 0.016 mmol) was carried as before for **NP1-IL**. EDX analysis on a single particle with ~14 nm diameter (*cf.* Fig. 4) (at.%) (*k*-factors: Ni: 1.511, Ga: 1.934): P1: Ni 71%; Ga 29% (±10–15% relative error), P2: Ni 71%; Ga 29% (±10–15% relative error), P3: Ni 71%; Ga 29% (±10–15% relative error).

Catalytic hydrogenation of alkynes

A Büchi stainless-steel autoclave with a glass inlet was charged with 0.1 g of a freshly synthesized NiGa/$[BMIm][BF_4]$ or Ni/$[BMIm][BF_4]$ dispersion (0.5 wt% in total metal, 85 μmol Ni or 39 μmol NiGa). 2 g of degassed, dry substrate 1-octyne (2.5 mL, 18.1 mmol) or phenylacetylene (tolan, 11.2 mmol) was added. For 1-octyne the NiGa : substrate ratio was 1 : 464 or Ni : substrate ratio = 1 : 212; NiGa : tolan = 1 : 287, Ni : tolan = 1 : 131. The reaction mixture was heated to 120 °C. After reaching the reaction temperature the autoclave was pressurized with H_2 to 5 bar (Büchi press flow gas controller, bpc) which was kept constant by the Büchi bpc. After the chosen time (3 h) the reaction was stopped, cooled down and a 0.5 g sample was analyzed for its content by GC/MS and NMR. Conversion and selectivity were determined by GC/MS (Tables S5 and S6 in the ESI†) [retention times: 1.51 (1-octene), 1.67 (octane), 1.87 (1-octyne), Shimadzu GC2014, column Ultra2, crosslinked 5% PhMe silicone, 25 m × 0.2 mm × 11 μm]. A ^1H NMR spectrum was recorded by dissolving 0.1 mL of the sample in 0.65 mL deuterated chloroform (see Fig. S21 in the ESI†).

Acknowledgements

Authors are thankful to the Deutsche Forschungsgemeinschaft (DFG) for financial support and to Dr. Juri Barthel and the Ernst Ruska-Centre (ER-C) for Microscopy and Spectroscopy with Electrons, Jülich Research Centre and RWTH Aachen University, 52425 Jülich, Germany for help and access to the TEM facilities.

Notes and references

1 (*a*) S. Duan and R. Wang, *Progress in Natural Science: Materials International*, 2013, **23**, 113–126, and references in there; (*b*) G. Krishnan, M. A. Verheijen, G. H. ten Brink, G. Palasantzas and B. J. Kooi, *Nanoscale*, 2013, **5**, 5375–5383; (*c*) J. H. Sinfelt, *J. Catal.*, 1973, **29**, 308–315; (*d*) J. H. Sinfelt, *Bimetallic Catalysts: Discoveries, Concepts and Applications*, Wiley, New York, 1983.

2 (*a*) F. Tao, S. Zhang, L. Nguyen and X. Zhang, *Chem. Soc. Rev.*, 2012, **41**, 7980–7993; (*b*) Y. Pei, G. Zhou, N. Luan, B. Zong, M. Qiao and F. Tao, *Chem. Soc. Rev.*, 2012, **41**, 8140–8162.

3 (*a*) M. Sankar, N. Dimitratos, P. J. Miedziak, P. P. Wells, C. J. Kiely and G. J. Hutchings, *Chem. Soc. Rev.*, 2012, **41**, 8099–8139; (*b*) D. M. Alonso, S. G. Wettstein and J. A. Dumesic, *Chem. Soc. Rev.*, 2012, **41**, 8075–8098; (*c*) R. Ferrando, J. Jellinek and R. L. Johnston, *Chem. Rev.*, 2008, **108**, 847–910; (*d*) M. Fatmi, M. A. Ghebouli, T. Chihi, S. Boucetta and Z. K. Heiba, *Rom. J. Phys.*, 2011, **56**, 935–951.

4 (*a*) J. Zhang, G. Chen, D. Guay, M. Chaker and D. Ma, *Nanoscale*, 2014, **6**, 2125–2130; (*b*) P. Xi, Y. Cao, F. Yang, C. Ma, F. Chen, S. Yu, S. Wang, Z. Zeng and X. Zhang, *Nanoscale*, 2013, **5**, 6124–6130; (*c*) F. Nosheen, Z.-C. Zhang, J. Zhuang and X. Wang, *Nanoscale*, 2013, **5**, 3660–3663; (*d*) Y. Li, Z. W. Wang, C.-Y. Chiu, L. Ruan, W. Yang, Y. Yang, R. E. Palmer and Y. Huang, *Nanoscale*, 2012, **4**, 845–851; (*e*) J. Liu, L. L. Zhang, J. Zhang, T. Liu and X. S. Zhao, *Nanoscale*, 2013, **5**, 11044–11050; (*f*) D. Cheng and W. Wang, *Nanoscale*, 2012, **4**, 2408–2415; (*g*) Z.-C. Zhang, J.-F. Hui, Z.-G. Guo, Q.-Y. Yu, B. Xu, X. Zhang, Z.-C. Liu, C.-M. Xu, J.-S. Gao and X. Wang, *Nanoscale*, 2012, **4**, 2633–2639; (*h*) S. Shen, J. Zhuang, Y. Yang and X. Wang, *Nanoscale*, 2011, **3**, 272–279.

5 (*a*) S. Khanal, N. Bhattarai, J. J. Velázquez-Salazar, D. Bahena, G. Soldano, A. Ponce, M. M. Mariscal, S. Mejía-Rosales and M. José-Yacamán, *Nanoscale*, 2013, **5**, 12456–12463; (*b*) P. Lara, O. R. Wheelaghan, S. Conejero, R. Poteau, K. Philippot and B. Chaudret, *Angew. Chem., Int. Ed.*, 2011, **50**, 12080–12084; (*c*) T. C. Golindano, S. I. Martínez, O. Z. Delgado and G. P. Rivas, *Nanotechnology*, 2005, **2**, 634–637; (*d*) N. Cordente, C. Amiens, B. Chaudret, M. Respaud and F. Senocq, *J. Appl. Phys.*, 2003, **94**, 6358–6365; (*e*) Y. Li, J. Liu, Y. Wang and Z. L. Wang, *Chem. Mater.*, 2001, **13**, 1008–1014.

6 B. Cormary, F. Dumestre, N. Liakakos, K. Soulantica and B. Chaudret, *Dalton Trans.*, 2013, **42**, 12546–12553.

7 (*a*) M. V. Kovalenko and C. Coperet, *Dalton Trans.*, 2013, **42**, 12520; (*b*) Ö. Metin, X. Sun and S. Sun, *Nanoscale*, 2013, **5**, 910–912; (*c*) C. Kumara and A. Dass, *Nanoscale*, 2012, **4**, 4084–4086; (*d*) Z.-C. Zhang, J.-F. Hui, Z.-G. Guo, Q.-Y. Yu, B. Xu, X. Zhang, Z.-C. Liu, C.-M. Xu, J.-S. Gao and X. Wang, *Nanoscale*, 2012, **4**, 2633–2639; (*e*) C. Kumara and A. Dass, *Nanoscale*, 2011, **3**, 3064–3067.

8 (*a*) M. Armbrüster, K. Kovnir, M. Behrens, D. Teschner, Y. Grin and R. Schlögl, *J. Am. Chem. Soc.*, 2010, **132**, 14745–14747; (*b*) M. Armbrüster, G. Wowsnick, M. Friedrich, M. Heggen and R. Cardoso-Gil, *J. Am. Chem. Soc.*, 2011, **133**, 9112–9118; (*c*) A. Ota, M. Armbrüster, M. Behrens, D. Rosenthal, M. Friedrich, I. Kasatkin and F. Girgsdies, *J. Phys. Chem. C*, 2011, **115**, 1368–1374; (*d*) M. Friedrich, D. Teschner, A. Knop-Gericke and M. Armbrüster, *J. Catal.*, 2012, **285**, 41–47; (*e*) K. Kovnir, M. Armbrüster, D. Teschner, T. Venkov, L. Szentmiklósi, F. C. Jentoft, A. Knop-Gericke, Yu. Grin and R. Schlögl, *Surface Sci.*, 2009, **603**, 1784–1792; (*f*) J. Osswald, K. Kovnir, M. Armbrüster, R. Giedigkeit, J. E. Jentoft, U. Wild, Y. Grin and R. Schlögl, *J. Catal.*, 2008, **258**, 219–227.

9 M. Armbrüster, K. Kovnir, M. Friedrich, D. Teschner, G. Wowsnick, M. Hahne, P. Gille, L. Szentmiklósi, M. Feuerbacher, M. Heggen, F. Girgsdies, D. Rosenthal, R. Schlögl and Yu. Grin, *Nat. Mater.*, 2012, **11**, 690–693.

10 (*a*) B. Bridier, J. Pérez-Ramírez, A. Knop-Gericke, R. Schlögl and D. Teschner, *Chem. Sci.*, 2011, **2**, 1379–1383; (*b*) B. Bridier and J. Pérez-Ramírez, *J. Am. Chem. Soc.*, 2010, **132**, 4321–4327.

11 (*a*) H. Arnold, F. Döbert and J. Gaube, in *Handbook of Heterogeneous Catalysis*, ed. G. Ertl, H. Knözinger and J. Weitkamp, VCH, Weinheim, 1997, p. 2165; (*b*) A. Borodzinski, *Catal. Rev.*, 2006, **48**, 91–144; (*c*) A. Borodzinski and G. C. Bond, *Catal. Rev.*, 2008, **50**, 379–469.

12 S. Dominguez-Dominguez, A. Berenguer-Murcia, D. Cazorla-Amoros and A. Linares-Solano, *J. Catal.*, 2006, **243**, 74–81.

13 (*a*) M. P. Conley, R. M. Drost, M. Baffert, D. Gajan, C. Elsevier, W. T. Franks, H. Oschkinat, L. Vyre, A. Zagdoun, A. Rossini, M. Lelli, A. Lesage, G. Casano, O. Ouari, P. Tordo, L. Emsley, C. Copéret and C. Thieuleux, *Chem.–Eur. J.*, 2013, **19**, 12234–12238; (*b*) T. Mitsudome, Y. Takahashi, S. Ichikawa, T. Mizugaki, K. Jitsukawa and K. Kaneda, *Angew. Chem., Int. Ed.*, 2013, **52**, 1481–1485; (*c*) P. Zhang, J. Yuan, T.-P. Fellinger, M. Antonietti, H. Li and Y. Wang, *Angew. Chem., Int. Ed.*, 2013, **52**, 6028–6032; (*d*) A. Yarulin, I. Yuranov, F. Cardenas-Lizana, P. Abdulkin and L. Kiwi-Minsker, *J. Phys. Chem. C*, 2013, **117**, 13424–13434; (*e*) D. Deng, Y. Yang, Y. Gong, Y. Li, X. Xu and Y. Wang, *Green Chem.*, 2013, **15**, 2525–2531.

14 P. T. Witte, S. Boland, F. Kirby, R. van Maanen, B. F. Bleeker, D. A. Matthijs de Winter, J. A. Post, J. W. Geus and P. H. Berben, *ChemCatChem*, 2013, **5**, 582–587.

15 G. A. Attard, J. A. Bennett, I. Mikheenko, P. Jenkins, S. Guan, S. L. E. Macaskie, J. Wood and A. J. Wain, *Faraday Discuss*, 2013, **162**, 57–75.

16 M. Niu, Y. Wang, W. Li, J. Jiang and Z. Jin, *Catal. Commun.*, 2013, **38**, 77–81.

17 D. Köhler, M. Heise, A. I. Baranov, Y. Luo, D. Geiger, M. Ruck and M. Armbrüster, *Chem. Mater.*, 2012, **24**, 1639–1644.

18 M. Yan, T. Jin, Y. Ishikawa, T. Minato, T. Fujita, L.-Y. Chen, M. Bao, N. Asao, M.-W. Chen and Y. Yamamoto, *J. Am. Chem. Soc.*, 2012, **134**, 17536–17542.

19 (*a*) D. Mei, M. Neurock and C. M. Smith, *J. Catal.*, 2009, **268**, 181–195; (*b*) Y. Jin, A. K. Datye, E. Rightor, R. Gulotty, W. Waterman, M. Smith, M. Holbrook, J. Maj and J. Blackson, *J. Catal.*, 2001, **203**, 292–306; (*c*) N. A. Khan, S. Shaikhutdinov and H.-J. Freund, *Catal. Lett.*, 2006, **108**, 159–163.

20 W. M. H. Sachtler, *Catal. Rev.: Sci. Eng.*, 1976, **14**, 193–197.

21 D. Teschner, J. Borsodi, A. Wootsch, Z. Révay, M. Hävecker, A. Knop-Gericke, S. D. David Jackson and R. Schlögl, *Science*, 2008, **320**, 86–89.

22 M. Cokoja, H. Parala, M. K. Schröter, A. Birkner, M. W. E. van den Berg, K. V. Klementiev, W. Grünert and R. A. Fischer, *J. Mater. Chem.*, 2006, **16**, 2420–2428.

23 K. Schütte, H. Meyer, C. Gemel, J. Barthel, R. A. Fischer and C. Janiak, *Nanoscale*, 2014, **6**, 3116–3126.

24 (*a*) M. Cokoja, H. Parala, A. Birkner, O. Shekhah, M. W. E. van den Berg and R. A. Fischer, *Chem. Mater.*, 2007, **19**, 5721–5733; (*b*) M. Cokoja, H. Parala, A. Birkner, R. A. Fischer, O. Margeat, D. Ciuculescu, C. Amiens, B. Chaudret, A. Falqui and P. Lecante, *Eur. J. Inorg. Chem.*, 2010, 1599–1603; (*c*) M. Cokoja, PhD thesis, Ruhr University Bochum, Germany, 2007; (*d*) A. Doddi, PhD thesis, Ruhr University Bochum, 2012.

25 (*a*) V. I. Pârvulescu and C. Hardacre, *Chem. Rev.*, 2007, **107**, 2615–2665; (*b*) J. D. Scholten, B. C. Leal and J. Dupont, *ACS Catal.*, 2012, **2**, 184–200.

26 (*a*) E. Redel, M. Walter, R. Thomann, L. Hussein, M. Krüger and C. Janiak, *Chem. Commun.*, 2010, **46**, 1159–1161; (*b*) E. Redel, M. Walter, R. Thomann, C. Vollmer, L. Hussein, H. Scherer, M. Krüger and C. Janiak, *Chem.–Eur. J.*, 2009, **15**, 10047–10059; (*c*) E. Redel, R. Thomann and C. Janiak, *Inorg. Chem.*, 2008, **47**, 14–16.

27 (*a*) G. S. Fonseca, G. Machado, S. R. Teixeira, G. H. Fecher, J. Morais, M. C. M. Alves and J. Dupont, *J. Colloid Interface Sci.*, 2006, **301**, 193–204; (*b*) G. S. Fonseca, J. B. Domingos, F. Nome and J. Dupont, *J. Mol. Catal. A: Chem.*, 2006, **248**, 10–16; (*c*) G. S. Fonseca, A. P. Umpierre, P. F. P. Fichtner, S. R. Teixeira and J. Dupont, *Chem.–Eur. J.*, 2003, **9**, 3263–3269; (*d*) J. Dupont, G. S. Fonseca, A. P. Umpierre, P. F. P. Fichter and S. R. Teixeira, *J. Am. Chem. Soc.*, 2002, **124**, 4228–4229.

28 (*a*) P. Arquillière, P. H. Haumesser and C. C. Santini, *Microelectron. Eng.*, 2012, **92**, 149–151; (*b*) E. T. Silveira, A. P. Umpierre, L. M. Rossi, G. Machado, J. Morais, G. V. Soares, I. J. R. Baumvol, S. R. Teixeira, P. F. P. Fichtner and J. Dupont, *Chem.–Eur. J.*, 2004, **10**, 3734–3740.

29 P. Migowski, G. Machado, S. R. Teixeira, M. C. M. Alves, J. Morais, A. Traverse and J. Dupont, *Phys. Chem. Chem. Phys.*, 2007, **9**, 4814–4821.

30 (*a*) D. Marquardt, J. Barthel, M. Braun, C. Ganter and C. Janiak, *CrystEngComm*, 2012, **14**, 7607–7615; (*b*) G. Salas, A. Podgorsek, P. S. Campbell, C. C. Santini, A. A. H. Pádua, M. F. Costa Gomes, K. Philippot, B. Chaudret and M. Turmine, *Phys. Chem. Chem. Phys.*, 2011, **13**, 13527–13536; (*c*) T. Gutel, J. Garcia-Antón, K. Pelzer, K. Philippot, C. C. Santini, Y. Chauvin, B. Chaudret and J.-M. Basset, *J. Mater. Chem.*, 2007, **17**, 3290–3292.

31 P. S. Campbell, M. H. G. Prechtl, C. C. Santini and P.-H. Haumesser, *Curr. Org. Chem.*, 2013, **17**, 414–429.

32 (*a*) C. Vollmer and C. Janiak, *Coord. Chem. Rev.*, 2011, **255**, 2039–2057; (*b*) C. Vollmer, M. Schröder, Y. Thomann, R. Thomann and C. Janiak, *Appl. Catal., A*, 2012, **425–426**, 178–183; (*c*) D. Marquardt, C. Vollmer, R. Thomann, P. Steurer, R. Mülhaupt, E. Redel and C. Janiak, *Carbon*, 2011, **49**, 1326–1332; (*d*) D. Marquardt, Z. Xie, A. Taubert, R. Thomann and C. Janiak, *Dalton Trans.*, 2011, **40**, 8290–8293; (*e*) C. Vollmer, E. Redel, K. Abu-Shandi, R. Thomann, H. Manyar, C. Hardacre and C. Janiak, *Chem.–Eur. J.*, 2010, **16**, 3849–3858; (*f*) E. Redel, J. Krämer, R. Thomann and C. Janiak, *J. Organomet. Chem.*, 2009, **694**, 1069–1075; (*g*) J. Krämer, E. Redel, R. Thomann and C. Janiak, *Organometallics*, 2008, **27**, 1976–1978; (*h*) E. Redel, R. Thomann and C. Janiak, *Chem. Commun.*, 2008, 1789–1791.

33 (*a*) C. Janiak, *Z. Naturforsch., B: J. Chem. Sci.*, 2013, **68**, 1059–1089; (*b*) D. Marquardt and C. Janiak, *Nachr. Chem.*, 2013, **61**, 754–757.

34 (*a*) L. S. Hsu, K. L. Tsang and S. C. Chung, *Mater. Res. Soc. Symp. Proc.*, 1996, **437**, 53–58; (*b*) S. Y. Lee and P. Nash, *Ga-Ni (Gallium-Nickel), Phase Diagrams of Binary Nickel Alloys*, ed. P. Nash, ASM International, Materials Park, OH, 1991, pp. 133–140; (*c*) T. Ikeda, Y. Nose, T. Korata, H. Numakura and M. Koiwa, *J. Phase Equilib. Diffus.*, 1999, **20**, 626–630; (*d*) R. Ducher, R. Kainuma and K. Ishida, *Intermetallics*, 2007, **15**, 148–153; (*e*) C. Schmetterer, H. Flandorfer, C. L. Lengauer, J. P. Bros and H. Ipser, *Intermetallics*, 2010, **18**, 277–285; (*f*) M. F. Singleton and P. Nash, *Bull. Alloy Phase Diagrams*, 1988, **9**, 592–597; (*g*) P. Waldner and H. Ipser, *Z. Metallkd.*, 2002, **93**, 825–832; (*h*) H. Okamoto, *J. Phase Equilib. Diffus.*, 2003, **24**, 379.

35 (*a*) K. P. Gupta, *J. Phase Equilib. Diffus.*, 2008, **29**, 101–109; (*b*) H. Okamoto, *J. Phase Equilib. Diffus.*, 2010, **31**, 575–576; (*c*) H. Okamoto, *J. Phase Equilib. Diffus.*, 2008, **29**, 296.

36 (*a*) A. Pramanick and X.-L. Wang, *JOM*, 2013, **65**, 54–64; (*b*) A. Backen, S. R. Yeduru, A. Diestel, L. Schultz, M. Kohl and S. Faehler, *Adv. Eng. Mater.*, 2012, **14**, 696–709; (*c*) K. V. Peruman and M. Mahendran, *Pure Appl. Chem.*, 2011, **83**, 2071–2077; (*d*) K. V. Peruman, M. Mahendran, S. Seenithurai, R. Chokkalingam, R. K. Singh and V. Chandrasekaran, *J. Phys. Chem. Solids*, 2010, **71**, 1540–1544.

37 (*a*) L.-S. Hsu, Y. D. Yao and Y. Y. Chen, *Mod. Phys. Lett. B.*, 1997, **11**, 407–414; (*b*) J. A. Leiro and M. H. Heinonen, *Surf. Sci.*, 1996, **346**, 73–78; (*c*) L. S. Hsu and R. S. Williams, *J. Phys. Chem. Solids*, 1994, **55**, 305–312; (*d*) T. J. Bastow and G. W. West, *J. Phys.: Condens. Matter*, 2003, **15**, 8389–8406.

38 (*a*) P. Lara, O. R. Wheelaghan, S. Conejero, R. Poteau, K. Philippot and B. Chaudret, *Angew. Chem., Int. Ed.*, 2011, **50**, 12080–12084; (*b*) T. C. Golindano, S. I. Martínez, O. Z. Delgado and G. P. Rivas, *Nanotechnology*, 2005, **2**, 634–637; (*c*) N. Cordente, C. Amiens, B. Chaudret, M. Respaud and F. Senocq, *J. Appl. Phys.*, 2003, **94**, 6358–6365.

39 (*a*) J. D. Makinson, J. S. Lee, S. H. Magner, R. J. De Angelis, W. N. Weins and A. S. Hieronymus, *Adv. X-Ray Anal.*, 2000, **42**, 407–411; (*b*) F. Zhang, S.-W. Chan, J. E. Spanier, E. Apak, Q. Jin, R. D. Robinson and I. P. Herman, *Appl. Phys. Lett.*, 2002, **80**, 127–129; (*c*) K. M. Reddy, S. V. Manorama and A. R. Reddy, *Mater. Chem. Phys.*, 2002, **78**, 239–245.

40 M. Molon, T. Bollermann, C. Gemel, J. Schaumann and R. A. Fischer, *Dalton Trans.*, 2011, **40**, 10769–10774.

41 L. S. Meriwether and M. L. Fiene, *J. Am. Chem. Soc.*, 1959, **81**, 4200–4208.

42 T. Welton, *Chem. Rev.*, 1999, **99**, 2071–2084.

43 J. P. Hallett and T. Welton, *Chem. Rev.*, 2011, **111**, 3508–3576.
44 (*a*) T. Torimoto, T. Tsuda, K. Okazaki and S. Kuwabata, *Adv. Mater.*, 2010, **22**, 1196–1221; (*b*) C. Feldmann, *Z. Naturforsch., B: J. Chem. Sci.*, 2013, **68**, 1057.
45 D. Freudenmann, S. Wolf, M. Wolff and C. Feldmann, *Angew. Chem., Int. Ed.*, 2011, **50**, 11050–11060.
46 (*a*) E. Ahmed, J. Breternitz, M. F. Groh and M. Ruck, *CrystEngComm*, 2012, **14**, 4874–4885; (*b*) E. Ahmed and M. Ruck, *Dalton Trans.*, 2011, **40**, 9347–9357; (*c*) M. F. Groh, U. Müller, E. Ahmed, A. Rothenberger and M. Ruck, *Z. Naturforsch., B: J. Chem. Sci.*, 2013, **68**, 1108–1122.
47 R. E. Morris, *Chem. Commun.*, 2009, 2990–2998.
48 E. R. Parnham and R. E. Morris, *Acc. Chem. Res.*, 2007, **40**, 1005–1013.
49 J. Dupont and J. D. Scholten, *Chem. Soc. Rev.*, 2010, **39**, 1780–1804.
50 Y. Lin and S. Dehnen, *Inorg. Chem.*, 2011, **50**, 7913–7915.
51 P. Lodge, *Science*, 2008, **321**, 50.
52 M. Larhed, C. Moberg and A. Hallberg, *Acc. Chem. Res.*, 2002, **35**, 717–727.
53 M. F. Groh, M. Heise, M. Kaiser and M. Ruck, *Nachr. Chem.*, 2013, **61**, 26–29.
54 A. L. Buchachenko and E. L. Frankevich, *Chemical Generation and Reception of Radio- and Microwaves*, Wiley-VCH, Weinheim, Germany, 1993, pp. 41–56.
55 V. K. Ahluwulia, *Alternative Energy Processes in Chemical Synthesis*, Alpha Science International LTD, Oxford, United Kingdom, 2008.
56 I. Bilecka and M. Niederberger, *Nanoscale*, 2010, **2**, 1358–1374.
57 J. I. Langford and A. J. C. Wilson, *J. Appl. Crystallogr.*, 1978, **11**, 102–113.
58 M. Cokoja, H. Parala, M. K. Schroter, A. Birkner, M. W. E. van den Berg, W. Grunert and R. A. Fischer, *Chem. Mater.*, 2006, **18**, 1634–1642.
59 J. D. Scholten, G. Ebeling and J. Dupont, *Dalton Trans.*, 2007, 5554–5560.
60 T. Cadenbach, C. Gemel, R. Schmid, M. Halbherr, K. Yusenko, M. Cokoja and R. A. Fischer, *Angew. Chem., Int. Ed.*, 2009, **48**, 3872–3876.
61 M. Treguer, C. de Cointet, H. Remita, J. Khatouri, M. Mostafavi, J. Amblard and J. Belloni, *J. Phys. Chem. B*, 1998, **102**, 4310–4321.
62 (*a*) F. Alonso, I. Osante and M. Yus, *Tetrahedron*, 2006, **63**, 93–102; (*b*) F. Alonso, I. Osante and M. Yus, *Adv. Synth. Catal.*, 2006, **348**, 305–308.
63 T. Steinke, M. Cokoja, C. Gemel, A. Kempter, A. Krapp, G. Frenking, U. Zenneck and R. A. Fischer, *Angew. Chem., Int. Ed.*, 2005, **44**, 2943–2946.
64 D. J. Krysan and P. B. Mackenzie, *J. Org. Chem.*, 1990, **55**, 4229–4230.
65 (*a*) P. Jutzi, B. Neumann, G. Reumann and H. G. Stammler, *Organometallics*, 1998, **17**, 1305–1314; (*b*) P. Jutzi and L. O. Schebaum, *J. Organomet. Chem.*, 2002, **654**, 176–179.